NANO LETTERS

2004
Vol. 4, No. 3
525−531

Efficient Inverse Auger Recombination at Threshold in CdSe Nanocrystals

Marco Califano and Alex Zunger*

National Renewable Energy Laboratory, Golden, Colorado 80401

Alberto Franceschetti

Oak Ridge National Laboratory, Oak Ridge, Tennessee 37831

Received January 21, 2004

ABSTRACT

We apply the semiempirical nonlocal pseudopotential method to the investigation of prospects for direct carrier multiplication (DCM) in neutral and negatively charged CdSe nanocrystals. In this process, known in the bulk as impact ionization, a highly excited carrier transfers, upon relaxation to the band edge, its excess energy Δ to a valence electron, promoting it across the band gap and thus creating two excitons from one. For excess energies just a few meV above the energy gap E_g (the DCM threshold), we find the following: (i) DCM is much more efficient in quantum dots than in bulk materials, with rates of the order of 10^{10} s^{-1}. In conventional bulk solids, comparable rates are obtained only for excess energies about 1 eV above E_g. (ii) Unlike the case in the bulk, in both neutral and charged nanocrystals the DCM rate is not an increasing function of the excess energy but oscillates as Δ moves in and out of resonance with the energy of the discrete spectrum of these 0D systems. (iii) The main contribution to the DCM rates is found to come from the dot surface, as in the case of Auger multiexciton recombination rates. (iv) Direct radiative recombination of excited electron–hole pairs and phonon-assisted decay are slower than DCM, but (v) the rate of Auger cooling (where the relaxation energy of an excited electron is used to excite a hole into deeper levels) can be of the same order of magnitude as that of the DCM process. Furthermore, for excess energies well above the DCM threshold, the presence of an energy gap within the hole manifold considerably slows DCM compared to Auger cooling (AC), which is not affected by it. Achieving competitive DCM processes will, therefore, require the suppression of Auger cooling, for example, by removing the hole from the dot or by trapping it at the surface.

Many optoelectronic devices could achieve much higher efficiencies if electrons excited well above the conduction-band minimum (CBM) did not lose their energy to thermal excitation of the lattice upon relaxation to the band edge but transferred it instead to other valence electrons, exciting them across the gap. It would then be possible to obtain two electron−hole pairs from a single photogenerated exciton (Figure 1, process 4). This effect could be beneficial to photovoltaic applications: by utilizing the excess energy of the photogenerated carriers to produce higher photocurrents, the maximum attainable thermodynamic conversion efficiency could conceivably increase from about 30% for a conventional single-absorber cell[1] up to 66%.[2] Furthermore, if this multiplication process were proven efficient, creating high-energy excitons ($h\nu \geq 2E_g$) could represent a more effective alternative to HOMO−LUMO pumping ($h\nu \geq E_g$) for achieving population inversion in the lasing process. In this letter, we calculate for the first time the probability of such a process in CdSe quantum dots, comparing it to the rates of possible competing decay channels.

If the excess energy of the electron $\Delta = h\nu - E_g$ is larger than the excitonic gap E_g (i.e., if the energy of the incident photon $h\nu$ is $>2E_{gap}$), then the hot electron can create one (or more) additional electron−hole pair(s) upon relaxation to the CBM through direct carrier multiplication (DCM), known in the bulk as impact ionization.[3−15] In this process, which is the inverse of Auger (multiexciton) recombination,[16,17] a highly excited carrier decays to its band edge and excites a valence electron across the band gap (process 1 or 4 in Figure 1). Because of the large confinement typical for quantum dots in the size range of a few nanometers, the Coulomb interaction between electron and hole is stronger compared to that in bulk materials[18,19] and is therefore expected to enhance DCM as it has been found to enhance Auger biexciton recombination and Auger processes in general.[17,20] Furthermore, as in quantum dots there is no momentum conservation (the wave vector momentum is not a "good" quantum number in 0D systems), the DCM threshold energy E_{th} is expected to equal[2] E_g. In bulk solids, instead, because of both energy and momentum conservation constraints,[7] $E_{th} = E_g + \delta E$, where δE varies from ∼0.1 eV for InAs[8] and ∼0.2 eV[9] or ∼0.3 eV[10] for GaAs to ∼1 eV for InP.[8] Despite all of these potential advantages over 3D systems, however, DCM rates have never been calculated for quantum dots. Effective-mass-based 8-band **k·p** methods

* Corresponding author. E-mail: alex_zunger@nrel.gov.

10.1021/nl049869w CCC: $27.50
Published on Web 02/14/2004

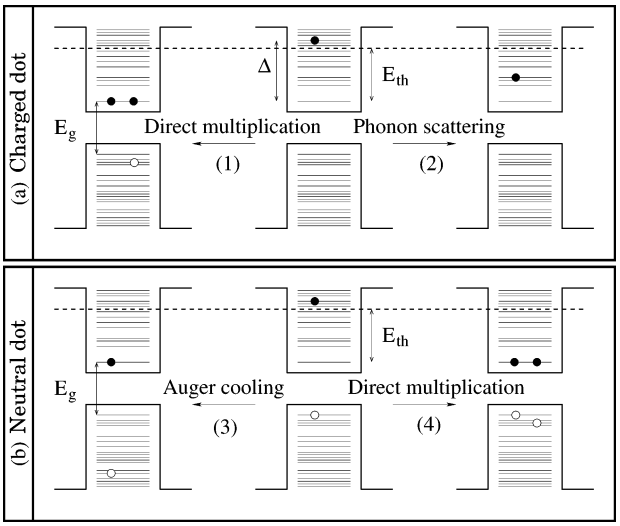

Figure 1. Schematics of hot electron relaxation pathways. (a) Charged dot: direct carrier multiplication (1) and phonon scattering (2). (b) Neutral dot: because of the presence of the hole, the AC process (3) represents an alternative decay mechanism to (1) and (2).

are clouded by uncertain wave functions, including the occurrence[21,22] of spurious gap levels and the need[23] for previously unrecognized[16,18,21] boundary conditions, demanding yet new adjustable parameters that are not supplied by the theory itself.[23] Furthermore, the **k·p** description of the highly excited states involved in DCM and Auger processes is not sufficiently accurate.[24] Indeed, a comparison of **k·p** and accurate pseudopotential cross sections for Auger cooling in CdSe dots showed[17] large discrepancies.

There are therefore many open questions: it is not known (i) whether the DCM process is actually more efficient in 0D dots than it is in 3D (bulk) systems, (ii) what the energy dependence of its rates is, and (iii) whether it can compete with alternative decay channels. Furthermore, (iv) which of the possible alternative decay mechanisms are most likely to be effectively competitive still remains to be determined. Because the details of the surface termination of experimentally synthesized nanoparticles may depend on the growth method, it is very important to determine the dependence of a specific process on the surface structure or, in other words, the origin (i.e., the dot interior or its surface) of the dominant contribution to the rates of each specific process. We address all of (but not only) these issues in this letter. We apply our semiempirical nonlocal pseudopotential method[25] to the investigation of the dependence on the electron excess energy of the DCM rates and of the rates of selected competing processes in negatively charged (Figures 3 and 4) and neutral (Figures 5 and 6) CdSe colloidal dots. To the best of our knowledge, this is the first time such rates have been calculated for a 0D structure. The computational approach we use was developed in a previous paper.[17] The present letter focuses on the application of such an approach to the investigation of novel physical processes and their potential for device applications.

Method. There are two types of nanocrystals: (a) colloidal nanocrystal quantum dots,[26] chemically synthesized in solution and typically containing hundreds of atoms, whose surface is passivated either by organic molecules (such as TOPO or TOP) or by a different semiconductor (such as ZnS) to remove surface states; (b) nanoclusters,[27] containing typically tens of atoms, whose bare surface (where unsaturated bonds may exist) can be heavily reconstructed or even amorphous. We consider a spherical dot of type (a), Cd_{232}-Se_{235} of diameter 29.2 Å with the wurtzite crystal structure, whose surface is saturated by ligand potentials.[28] The single-particle energy levels ε_i are computed, in a supercell model, with the plane-wave semiempirical nonlocal pseudopotential method described in ref 25. The total pseudopotential of the system[29] includes a local part, which is obtained as a superposition of screened atomic potentials, and a nonlocal part, which accounts for spin−orbit coupling. The Hamiltonian is diagonalized by the order-N folded spectrum method.[30] Electron and hole levels are labeled with increasing and decreasing energy as e_i and h_j, respectively, with $i, j = 1, 2,...$, where $e_1 = e_{cbm}$ and $h_1 = h_{vbm}$. The DCM threshold energy E_{th} is defined as the energy below which no DCM can take place. However, because of the discrete nature of the energy spectrum in 0D structures, the condition $\varepsilon_{e_i} = E_{th}$ is never satisfied for the dot size considered. We label the electron states above the DCM threshold as e_{th+i}, where $i = 1, 2,...$ increases with energy. Figure 2 shows schematically our calculated single-particle energy levels for a $d = 29.2$-Å CdSe dot. Important features that will affect the calculation of DCM rates are the following: (a) The single-particle band gap (and therefore the DCM threshold E_{th}) is $E_g = 2.513$ eV. (b) The lowest (s-like) electron level e_1 is 412 meV below the second (p-like) level e_2. The s−p splitting is therefore much larger than the typical LO phonon energy in bulk CdSe (26 meV). (c) The energy spacings between e_{th+i} and e_{th+i+1} range from 1 to 20 meV (i.e., smaller than $\hbar\omega_{LO}$). (d) The first four hole levels below the band edge are spread over 56 meV, after which there is a large gap (∼130 meV) between levels h_4 and h_5.

DCM and AC rates are derived under the standard time-dependent perturbation theory.[17,31] The DCM rate for the process $e_{(th+i)} + h_1 \rightarrow 2e_1 + h_1 + h_n$ is calculated according to

$$R_{DCM}(E_i) = \frac{\Gamma}{\hbar}\sum_n \frac{|M(e_1, e_1; e_{th+i}, h_n)|^2}{(\varepsilon_{e_{th+i}} - E_g - \Delta_{n,1})^2 + (\Gamma/2)^2} \qquad (1)$$

where $\Delta_{n,1} = \varepsilon_{h_1} - \varepsilon_{h_n}$, and $\varepsilon_{e_{th+i}}$ (as throughout the paper) is measured from the CBM energy ε_{e_1}. The matrix element $M = M_d - M_e$ includes the direct part M_d, given by[17,31]

$$M_d(e_j, e_k, e_l, h_m) = \sum_{\sigma,\sigma'}\int\int \phi^*_{e_j}(\boldsymbol{r}, \sigma)\, \phi^*_{e_k}(\boldsymbol{r}', \sigma')\frac{e^2}{\bar{\epsilon}(\boldsymbol{r}, \boldsymbol{r}')|\boldsymbol{r} - \boldsymbol{r}'|} \times \phi_{e_l}(\boldsymbol{r}, \sigma)\phi_{h_m}(\boldsymbol{r}', \sigma')\, d^3r\, d^3r' \qquad (2)$$

and the exchange matrix element M_e obtained from eq 2 by

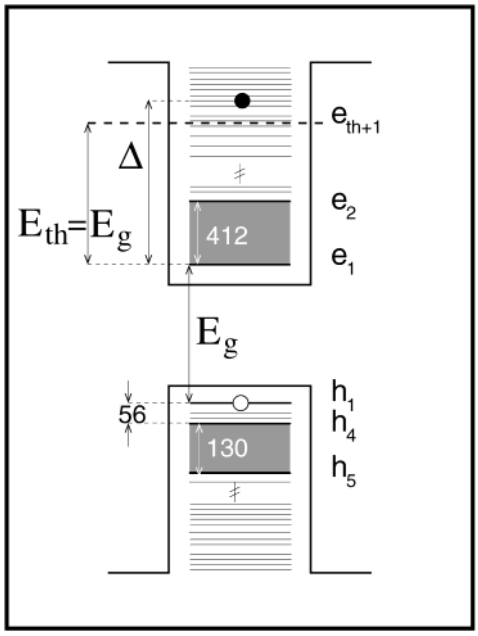

Figure 2. Schematics of single-particle electronic levels in a $d = 29.2$-Å CdSe dot. Large energy gaps are shown as gray areas. Energy separations are given in meV.

exchanging indices j and k. Here, $\{\phi_{e_i}\}$ ($\{\phi_{h_j}\}$) are the electron (hole) single-particle wave functions, and $\bar{\epsilon}(\boldsymbol{r}, \boldsymbol{r}')$ is the dielectric function of the dot. The AC rate for the decay $e_i + h_1 \rightarrow e_1 + h_n$ of an excited electron from state e_i to the ground state e_1 and the excitation of a hole from the ground state h_1 to a deep state h_n is given by[16,17]

$$R_{AC}(E_i) = \frac{\Gamma}{\hbar} \sum_{n,\alpha} \frac{|M_d(h_1, e_i, h_n, e_{1,\alpha})|^2}{(\varepsilon_{e_{th+i}} - E_g - \Delta_{n,1})^2 + (\Gamma/2)^2} \qquad (3)$$

where the sum runs over the spin $\alpha = \uparrow, \downarrow$ of the ground-state electron as well. In eqs 1 and 3, we sum over multiple final states $\{n\}$ (where n includes spin degrees of freedom as well). For $T \neq 0$, we take a Boltzmann average over the initial states because photogenerated (or injected) carriers thermalize (i.e., form thermal distributions described by Boltzmann statistics) in less than 100 fs.[32] We use the dielectric screening function[17]

$$\frac{1}{\bar{\epsilon}(\boldsymbol{r}, \boldsymbol{r}')} = [1 - m(r)\, m(r')] + \frac{m(r)\, m(r')}{\bar{\epsilon}_{in}(\boldsymbol{r}, \boldsymbol{r}')} \qquad (4)$$

where $m(r)$ is a mask function that changes smoothly from 1, when r is inside the dot, to 0, when r is outside. $\bar{\epsilon}(\boldsymbol{r}, \boldsymbol{r}')$, therefore, is equal to $\bar{\epsilon}_{in}(\boldsymbol{r}, \boldsymbol{r}')$ inside the dot and is equal to 1 when $\boldsymbol{r}$ or $\boldsymbol{r}'$ or both are outside the dot. In eq 4, the total screening is decomposed into its surface (term in square brackets) and volume (second term) contributions. This form allows us to write the integrals in eq 2 as $M = M^{surf} + M^{vol}$ and will be used to investigate the origins (dot surface or interior) of the dominant contribution to M and hence to DCM. This determination is of great importance. In fact, if the DCM rates originate mainly from the wave function portion close to the dot center (dot interior), then the quality of the dot surface (whether perfectly passivated or not) will not affect the total rate. If, instead, the main contribution is found to come from the dot surface, then the details of the surface termination may have a larger effect on DCM processes. For $\bar{\epsilon}_{in}(\boldsymbol{r}, \boldsymbol{r}')$, we use the dielectric screening of ref 29, which consists of an electronic and an ionic contribution approximated by the Thomas−Fermi model of Resta[33] and by the polaronic model of Haken,[34] respectively.

In actual nanocrystals, shape and size distributions, surface effects, and the presence of external charges near the dot can affect the relative positions of $\varepsilon_{e_{th+i}}$ and E_{th}. To simulate these effects, for each initial state e_{th+i} we keep the value of E_{th} fixed at E_g and vary $\varepsilon_{e_{th+i}}$ around the value ($\varepsilon^0_{e_{th+i}}$) calculated for a spherical dot with $d = 29.2$ Å. DCM and AC rates are thus calculated as a function of $\varepsilon_{e_{th+i}}$. (See Figures 3 and 5, where for illustrative purposes, we show a larger energy variation than expected from realistic effects. The position of $\varepsilon^0_{e_{th+i}}$ is marked by an arrow.) We then take an average[35] around $\varepsilon^0_{e_{th+i}}$ over an energy range corresponding to a 5% variation of the dot size (as determined by the variation of ε_{e_1} for the same size variation) of the DCM rate as a function of Δ calculated for every single level e_{th+i} and plot it as a function of the excess energy measured from E_g, as shown in Figures 4 and 6.

Results. There are two possible carrier configurations in which DCM can take place in a dot: (I) a charged dot, prepared with a single electron and no hole (Figure 1a); (II) a neutral dot with a photogenerated electron−hole pair (Figure 1b). In case (I), the only mechanism competing with DCM is phonon scattering (process 2 in Figure 1a), whereas in (II), because of the presence of the hole, Auger cooling (process 3 in Figure 1b) and radiative recombination also have to be taken into account. We do not calculate phonon scattering rates. Their determination is difficult even in the bulk where most of the time the ratio between phonon and impact ionization rates is treated as a fitting parameter[7−9,14] and is adjusted to reproduce impact ionization experimental results. Unfortunately, there are no experimental data available yet for DCM in dots; therefore, there is no easy way to estimate phonon scattering rates in these systems. To asses the likelihood of phonon cooling, however, we calculated energy levels $\{e_{th+i}\}$ above and $\{e_{th-j}\}$ below E_{th} and found that no spacing $\varepsilon_{e_{th+i}} - \varepsilon_{e_{th-j}}$ matched $\hbar\omega_{LO}$, the mismatches ranging from 10% for e_{th+3} to ∼50% for e_{th+1}. We therefore expect LO phonon-assisted decay rates between $\{e_{th+i}\}$ and $\{e_{th-j}\}$ (i.e., the rates of the only processes that, connecting states above the DCM threshold with states below it, effectively compete with DCM) to be small. As for direct radiative recombination, we find that its lifetimes (in the range of 10 s to 4 μs, depending on the excited electron state considered) are never comparable to those relative to either AC or DCM. In what follows, we discuss our results for the DCM rates in the two types of carrier configurations.

DCM in a Dot Charged with a Single Electron (Case I) (Figure 1a). We investigated DCM rates in two different ranges: (i) the electron energy $\varepsilon_{e_{th+i}}$ is just above threshold

(i.e., $\varepsilon_{e_{th+i}} \approx E_{th} = E_g$); (ii) $\varepsilon_{e_{th+i}}$ is well above threshold. Condition (i) corresponds to situations where the excess energy Δ is only enough to excite a valence electron from a state close to the band edge (h_1−h_4) into e_1. In case (ii), instead, Δ is sufficiently large that valence electrons can be promoted both from deep states to e_1 and from states close to the band edge to high conduction states (e_j, $j = 2, 3, 4$).

(i) DCM Rates at Threshold. We consider electron initial states $\{e_{th+i}\}$ with energies $\varepsilon_{e_{th+i}}$ ranging from just above E_{th} to $E_{th} + 60$ meV. We then take into account the possibility that the decaying electron will create an electron−hole pair that can be either in the ground state or in an excited state. The electron is always created in the ground state, e_1 (because the next electron state is more than 400 meV higher in energy, see Figure 2, and a transition from any $\{h_m\}$ to e_2 could not conserve energy), whereas the hole can be created in any of the states $\{h_m\}$ ($m = 1,...., 4$) within 56 meV from h_1 (the next hole state h_5 is ∼130 meV away from h_4,[36] Figure 2). The existence of such a large gap in the valence states between levels h_4 and h_5 is a feature common to spherical dots and was both detected experimentally[37] and predicted theoretically.[36] We find the following:

(a) The DCM rate is already of the order of 10^{10} s^{-1} for energies just a few meV above $E_{th} = E_g$ (Figure 3), whereas in conventional bulk materials (GaAs, $In_{0.53}Ga_{0.47}As$, and $Si_{0.5}Ge_{0.5}$, for example), values of that order of magnitude are reached only for energies ∼1 eV above E_g.[10] This represents a great improvement over the performance of bulk solids.

(b) The largest contribution (by about 1 order of magnitude) to DCM rates comes from the dot surface, as in the case of Auger multiexciton recombination lifetimes.[17] This is shown in Figure 3b, where the total DCM rate, calculated at room temperature for $\Gamma = 10$ meV,[38] is decomposed into surface and volume contributions.[40] Because we assume the dot surface to be perfectly crystalline and perfectly passivated, the calculated DCM rates may be different for a different surface termination.

(c) For all values of the temperature T (Figure 3a), the peaks of the DCM rate occur at energies in resonance with the transitions $h_m \rightarrow e_1$ ($m = 1, 2, 3$). With increasing T, higher states included in the Boltzmann average contribute to the DCM rate (peak on the low-energy side).

(d) Unlike in the bulk, where the impact ionization rate is an increasing function of Δ,[8−10] the DCM rate in a dot oscillates (Figure 3) depending on whether Δ is in or out of resonance with one of the possible transitions $h_j \rightarrow e_i$ of the discrete energy spectrum of the dot.

(e) Different transitions $h_j \rightarrow e_i$ have different contributions to DCM rates. In Figure 4, for example, the DCM rate is high for energies close to $E_{th} = \varepsilon_{e_1} - \varepsilon_{h_1}$, and it decreases when Δ increases, moving away from the resonance with $h_1 \rightarrow e_1 = E_{th}$. The DCM rate, then, increases again when Δ gets close to resonance with the energy of the transition $h_2 \rightarrow e_1 = E_{th} + 28$ meV (second arrow) and decreases again away from it. After that, it does not increase again even close to the next two resonances, indicating that the matrix elements for these transitions are smaller than those relative to the first two.

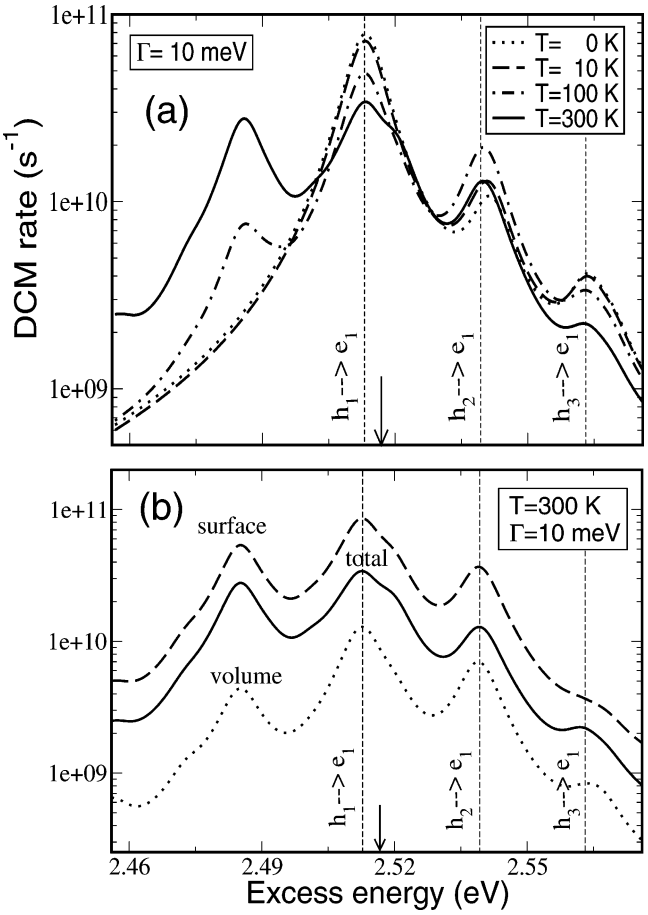

Figure 3. DCM rates (for $\Gamma = 10$ meV) for a CdSe dot charged with a single electron in e_{th+1} as a function of the excess energy Δ. Here, Δ is varied around the excess energy $\varepsilon^0_{e_{th+1}}$ calculated for a spherical dot with $d = 29.2$ Å (marked by the arrow) and presented (a) for four different values of the temperature T and (b) decomposed into surface (dashed line) and volume (dotted line) contributions[40] at room temperature. The dashed vertical lines mark the positions of the transitions $h_m \rightarrow e_1$, with $m = 1, 2, 3$.

(f) The DCM rate is rather insensitive to the exact value of the broadening parameter Γ.

(ii) DCM Rates for Excess Energies Well Above Threshold. When the excess energy $\Delta - E_g$ becomes larger than the energy difference between the e_1 and e_2 levels (∼400 meV for the dot size considered, see Figure 2), valence electrons can be promoted both from deep states $\{h_{m'}\}$ to e_1 and from states $\{h_m\}$ close to the band edge to high conduction states (e_j, $j = 2, 3, 4$). The DCM rate is therefore expected to increase in this energy range because of the increased number of final states available for the process. We find the contribution of $h_{m'} \rightarrow e_1$ transitions to be negligible compared to that of $h_m \rightarrow e_j$ transitions, even at resonance. Transitions involving conduction and valence states close to the band edges are found to have larger matrix elements than those relative to transitions between deep hole states and e_1 because of the different degree of localization (and therefore of overlap) of the respective wave functions. As a result, no dramatic increase in the DCM rates is found: they are of the same order of magnitude as those in case (i).

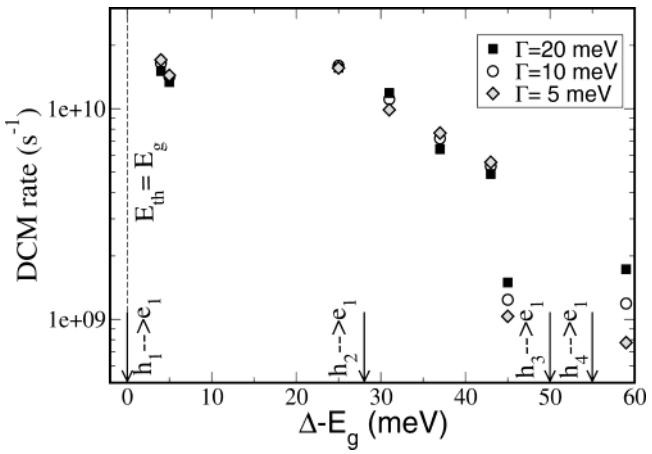

Figure 4. DCM average rates at room temperature for a $d = 29.2$ Å CdSe dot charged by a single electron in a level e_{th+i} as a function of its excess energy $\Delta - E_g$ calculated for eight different electron levels and for three values of the broadening parameter Γ. Each symbol is obtained as the average around $\varepsilon^0_{e_{th+i}}$, over an energy range corresponding to a 5% variation of the dot size, of the DCM rate as a function of Δ calculated for every single level e_{th+i}. The dashed vertical line indicates the value of E_{th} (relative to the transition $e_1 \rightarrow h_1$), whereas the arrows mark the positions in energy of the next possible transitions: $h_j \rightarrow e_1$ ($j = 2, 3, 4$).

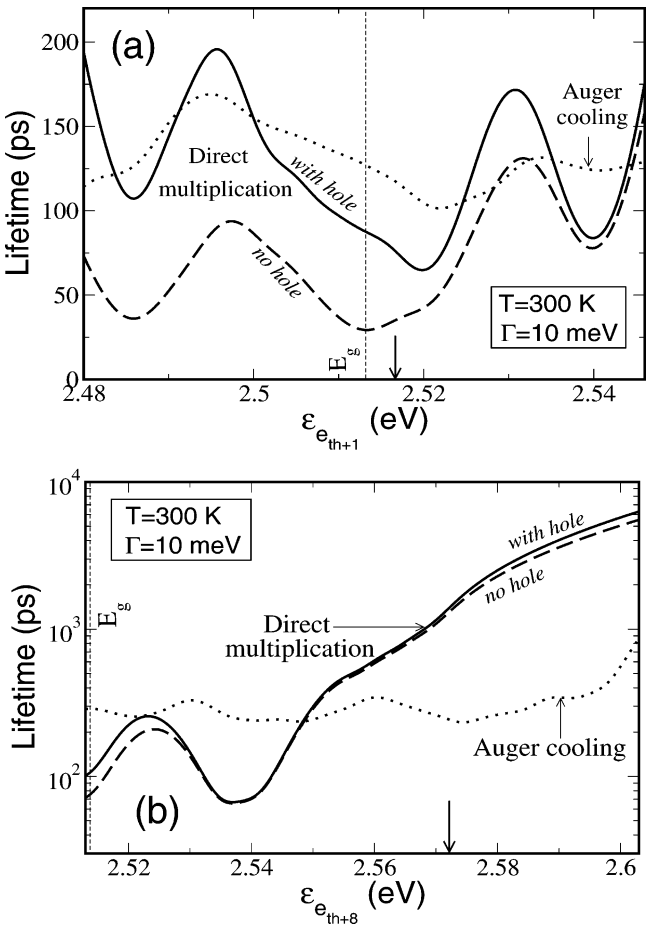

Figure 5. DCM and AC lifetimes (at room temperature and for $\Gamma = 10$ meV) for an electron with excess energy (a) just above E_{th} ($\varepsilon_{e_{th+1}}$) and (b) 60 meV above E_{th} ($\varepsilon_{e_{th+8}}$) in a neutral (solid and dotted lines) and a negatively charged (dashed lines) CdSe dot as a function of the excess energy $\varepsilon_{e_{th+i}} = h\nu - E_g$. $\varepsilon_{e_{th+i}}$ is varied around $\varepsilon^0_{e_{th+i}}$ (i.e., the value calculated for a spherical nanocrystal with $d = 29.2$ Å marked by the arrow).

Direct Carrier Multiplication by an Electron in the Presence of a Hole (Case II) (Figure 1b). To allow a comparison with case I above, we consider photogenerated electron−hole pairs where the electron occupies a level e_{th+i} ($i = 1,..., 8$) and the hole occupies the state at the top of the valence band. This configuration can either be generated directly by the absorption of photons with energies $h\nu_i = 2E_g + \delta\varepsilon_i$ (with $\delta\varepsilon_i = 4-60$ meV), in which case all excess energy $h\nu_i - E_g = E_g + \delta\varepsilon_i$ is given to the electron whereas the hole has no kinetic energy (a typical scenario, for example, in $Si_{0.32}Ge_{0.68}$ for $h\nu = 2E_g$[14,15]) or it can be the result of a higher-energy excitation. In the latter case, the excess energy $h\nu_i - E_g$ might be distributed between the electron and the hole. However, as the hole relaxes to the top of the valence band with characteristic times that are much smaller than our calculated DCM lifetimes, we can safely assume it to occupy its ground state in our initial DCM configuration. For DCM calculations, we consider the same states and follow the same procedure as we did in the case of the charged dot. The AC lifetimes are obtained by summing over 30 hole final states $\{h_{mi}\}$ whose energies are centered around $\varepsilon_{h_1} - E_g$. We find the following:

(a) For excess energies $\Delta = \varepsilon_{e_{th+i}} \approx E_{th}$ (Figure 5a), the DCM lifetime calculated in the presence of a hole is about a factor of 2 larger than that computed without it, both on average ($\langle\tau^{(w.h)}_{DCM}\rangle = 122$ ps, $\langle\tau^{(noh)}_{DCM}\rangle = 74$ ps) and at the position of the arrow [$\tau^{(w.h)}_{DCM}(\downarrow) = 76$ ps, $\tau^{(noh)}_{DCM}(\downarrow) = 35$ ps]. When a (photogenerated) hole is in its ground state, in fact, the number of final states $|h_m, e_1\rangle$ available to the e−h pair created via DCM is reduced. This leads to an increase in the lifetime compared to that of the configuration with no hole.

(b) Both DCM (with a hole) and AC lifetimes are of about the same order of magnitude, ∼100 ps, for excess energies $\Delta \approx E_{th}$. The DCM process is, however, slightly faster, with an average lifetime of 122 ps compared to the AC average lifetime of 132 ps. But more importantly, the DCM lifetime with a hole is about 2/3 of τ_{AC} at the arrow, yielding a DCM efficiency of 61% for the value of $\varepsilon_{e_{th+i}} - E_g$ calculated for this specific dot size.

(c) The presence of a hole in h_1 has a much smaller effect on the DCM lifetime for higher excess energies ($\varepsilon_{e_{th+8}}$), as shown in Figure 5b. This occurs because in this case the energy of the electron is (∼60 meV) larger than the energy of the transition $h_1 \rightarrow e_1$. Therefore, the reduction of the corresponding matrix element due to the presence of a "spectator" hole in h_1 does not appreciably affect the DCM lifetime because that matrix element is weighed by the energy difference between the initial and final states (eq 1) and the final state closest in energy to $\varepsilon_{e_{th+8}}$ corresponds to the transition $h_4 \rightarrow e_1$.

(d) When the electron is photogenerated on a level with energy higher than $E_g + 56$ meV (such as e_{th+8} in Figure 5b), AC will prevent efficient DCM. This is a consequence of the presence of an energy gap within the hole manifold (which, for a dot with $d = 29.2$ Å, is located 56 meV below

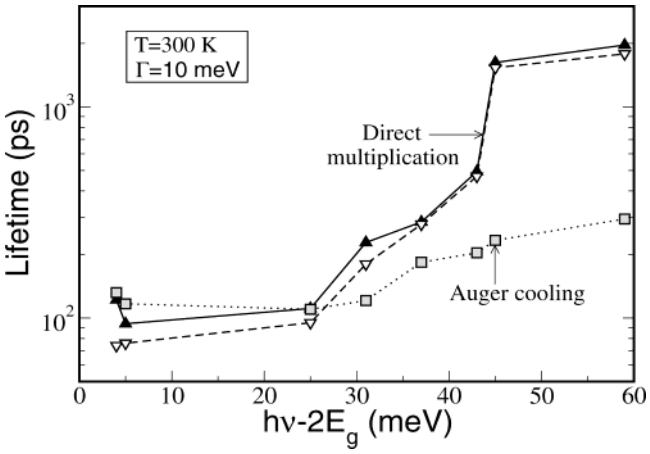

Figure 6. DCM average lifetimes with (filled triangles and solid line) and without (open triangles and dashed line) a hole present compared to Auger cooling average lifetimes (filled squares and solid line) for different initial electron levels e_{th+i} in a (both neutral and negatively charged) $d = 29.2$ Å CdSe nanocrystal as a function of the photon excess energy $h\nu - 2E_g$, as measured from E_g, at room temperature. Each symbol is obtained as the average around $\varepsilon^0_{e_{th+i}}$, over an energy range corresponding to a 5% variation of the dot size, of the DCM and Auger lifetimes as a function of $\varepsilon_{e_{th+i}}$, calculated for every single level e_{th+i}.

the VBM, see Figure 2) found[36] in spherical dots between levels h_4 and h_5: in that energy range, there are no energy-conserving transitions $h_n \rightarrow e_i$ available to the DCM process; the next transition $h_5 \rightarrow e_1$ is more than 100 meV higher in energy (Figure 2). Instead, such a gap does not exist within deep hole states (the ones involved in the AC process); therefore, the AC lifetime is almost constant for all energies. As a consequence, τ_{DCM}, which is smaller than τ_{AC} for excess energies up to 25 meV above E_g (Figure 6), becomes more than 1 order of magnitude larger than the AC lifetime for photon energies above the $h_4 \rightarrow e_1$ transition but below the $h_5 \rightarrow e_1$ transition. It follows that a natural way to enhance the DCM process relative to AC would be the introduction of a fast hole-trapping species whereby the hole is removed from the dot core and is trapped at its surface, leading to a suppression of the Auger cooling mechanism.

Decay of DCM Products. Because of the potential technological interest in carrier multiplication, we now briefly discuss the possible evolution of the system after DCM takes place, namely, the lifetime of the product of DCM (e.g, the biexciton or the trion). The most effective decay channel for the DCM final state (biexciton or charged exciton) is Auger recombination. It has been shown both theoretically[17] and experimentally[20] that the lifetime of the biexciton, due to Auger recombination of one of the two electron−hole pairs, is of the order of 5 ps for the dot size considered here. Likewise, the lifetime of a negative trion due to the Auger recombination of one of its electron−hole pairs has been calculated[17] to be of the order of 10 ps. The reason for such fast recombinations is that in CdSe dots the density of single-particle states at high electron energies is much higher than the DOS near the band edge. It follows that, unless externally prevented, the final state of the DCM process (biexciton or trion) will rapidly revert to the initial state (a single excited exciton or electron) from which it originated. Therefore, to take advantage of the efficiency of the DCM process at threshold, one has to devise a way to delay or suppress direct Auger recombination of the ensuing biexciton or trion. This could be achieved, for instance, through a fast separation of the carriers before direct Auger recombination can take place.

In summary, we calculated the rates of DCM and of selected competing processes in CdSe colloidal dots using our semiempirical pseudopotential approach. We found carrier multiplication rates that were much higher than in conventional bulk materials for electron excess energies just above the energy gap E_g. For a dot populated by a single electron−hole pair, among the possible competing mechanisms (phonon scattering, direct radiative recombination, and AC) the only process with decay rates comparable to those of DCM is found to be Auger cooling, which is, however, slower than DCM for excess energies a few meV above E_{th}. Our work therefore proves that exciting electrons in this energy range is a very efficient way to achieve population inversion in CdSe nanocrystals. For high excess energies, instead, the presence of an energy gap within the hole manifold close to the band edge slows DCM considerably compared to AC (that involving only deep hole states is unaffected by it), leading to inefficient carrier multiplication for excess energies in a window of the size of such a gap.

For both DCM and AC, transitions involving states close to the band edges were found to have larger matrix elements than those between highly excited states and s electron states. As in the case of Auger multiexciton recombination rates, for all excess energies the main contribution to the DCM rates was found to come from the dot surface. The details of the surface termination of the actual experimental samples may therefore affect the values of the DCM rates, which may be different for different degrees of passivation.

Acknowledgment. This work was supported by the U.S. DOE, OER-BES, Division of Materials Science, under the Nanoscience Initiative DOE LAB 03-17.

References

(1) Shockley, W.; Queisser, H. J. *J. Appl. Phys.* **1961**, *32*, 510.
(2) Nozik, A. J. *Physica E* **2002**, *14*, 115.
(3) Kolodinski, S.; Werner, J. H.; Wittchen, T.; Queisser, H. J. *Appl. Phys. Lett.* **1993**, *63*, 2405. Kolodinski, S.; Werner, J. H.; Queisser, H. J. *Sol. Energy Mater. Sol. Cells* **1994**, *33*, 275. Werner, J. H.; Kolodinski, S.; Queisser, H. J. *Phys. Rev. Lett.* **1994**, *72*, 3851. Werner, J. H.; Brendel, R.; Queisser, H. J. *Appl. Phys. Lett.* **1995**, *67*, 1028. Brendel, R.; Werner, J. H.; Queisser, H. J. *Sol. Energy Mater. Sol. Cells* **1996**, *41/42*, 419.
(4) Landsberg, P. T.; Nussbaumer, H.; Willeke, G. *J. Appl. Phys.* **1993**, *74*, 1451. Liakos, J. K.; Landsberg, P. T. *Semicond. Sci. Technol.* **1996**, *11*, 1895.
(5) Spirkl, W.; Ries, H. *Phys. Rev. B* **1995**, *52*, 11319.
(6) De Vos, A.; Desoete, B. *Sol. Energy Mater. Sol. Cells* **1998**, *51*, 413.
(7) Alig, R. C.; Bloom, S.; Struck, C. W. *Phys. Rev. B* **1980**, *22*, 5565.
(8) Bude, J.; Hess, K. *J. Appl. Phys.* **1992**, *72*, 3554.
(9) Jung, H. K.; Taniguchi, K.; Hamaguchi, C. *J. Appl. Phys.* **1996**, *79*, 2473.
(10) Harrison, D.; Abram, R. A.; Brand, S. *J. Appl. Phys.* **1999**, *85*, 8178. Harrison, D.; Abram, R. A.; Brand, S. *J. Appl. Phys.* **1999**, *85*, 8186.
(11) Lappe, F. *J. Phys. Chem. Solids* **1961**, *20*, 173.
(12) Klein, C. A. *J. Appl. Phys.* **1968**, *39*, 2029.

(13) Alig, R. C.; Bloom, S. *Phys. Rev. Lett.* **1975**, *35*, 1522.
(14) Wolf, M.; Brendel, R.; Werner, J. H.; Queisser, H. J. *J. Appl. Phys.* **1998**, *83*, 4213.
(15) Kolodinski, S.; Werner, J. H.; Queisser, H. J. *Appl. Phys. A* **1995**, *61*, 535.
(16) Efros, Al. L.; Kharchenko, V. A.; Rosen, M. *Solid State Commun.* **1995**, *93*, 281.
(17) Wang, L.-W.; Califano, M.; Zunger, A.; Franceschetti, A. *Phys. Rev. Lett.* **2003**, *91*, 056404.
(18) Chepic, D.; Efros, Al. L.; Ekimov, A.; Ivanov, M.; Kharchenko, V. A.; Kudriavtsev, I. *J. Lumin.* **1990**, *43*, 113.
(19) Bockelmann, U.; Egeler, T. *Phys. Rev. B* **1992**, *46*, 15574.
(20) Klimov, V. I.; Mikhailovsky, A. A.; McBranch, D. W.; Leatherdale, C. A.; Bawendi, M. G. *Science* **2000**, *287*, 1011.
(21) Sercel, P. C.; Efros, A. L.; Rosen, M. *Phys. Rev. Lett.* **1999**, *83*, 2394.
(22) Wang, L.-W. *Phys. Rev. B* **2000**, *61*, 7241. Wang, L. W.; Williamson, A. J.; Zunger, A.; Jiang, H.; Singh, J. *Appl. Phys. Lett.* **2000**, *76*, 339.
(23) Rodina, A. V.; Alekseev, A. Yu.; Efros, Al. L.; Rosen, M.; Meyer, B. K. *Phys. Rev. B* **2002**, *65*, 125302.
(24) Wang, L.-W.; Zunger, A. *J. Phys. Chem. B* **1998**, *102*, 6449.
(25) Wang, L.-W.; Zunger, A. *Phys. Rev. B* **1995**, *51*, 17398.
(26) Murray, C. B.; Norris, D. J.; Bawendi, M. G. *J. Am. Chem. Soc.* **1993**, *115*, 8706.
(27) Troparevsky, M. C.; Chelikowsky, J. R. *J. Chem. Phys.* **2001**, *114*, 943.
(28) Wang, L.-W.; Zunger, A. *Phys. Rev. B* **1996**, *53*, 9579.
(29) Franceschetti, A.; Fu, H.; Wang, L.-W.; Zunger, A. *Phys. Rev. B* **1999**, *60*, 1819.
(30) Wang, L.-W.; Zunger, A. *J. Chem. Phys.* **1994**, *100*, 2394.
(31) Landsberg, P. T. *Recombination in Semiconductors*; Cambridge University Press: Cambridge, England, 1991.
(32) Pelouch, W. S.; Ellingson, R. J.; Powers, P. E.; Tang, C. L.; Szmyd, D. M.; Nozik, A. J., *Phys. Rev. B* **1992**, *45*, 1450. Pelouch, W. S.; Ellingson, R. J.; Powers, P. E.; Tang, C. L.; Szmyd, D. M.; Nozik, A. J. *Semicond. Sci. Technol. B* **1992**, *7*, 337.
(33) Resta, R. *Phys. Rev. B* **1977**, *16*, 2717.
(34) Haken, H. *Lett. Nuovo Cimento* **1956**, *10*, 1230.
(35) The results obtained by taking only the value at $\varepsilon^0_{e_{th+i}}$ of the DCM rate versus Δ curve are of the same order of magnitude and exhibit the same behaviour as their average.
(36) Califano, M.; Bester, G.; Zunger, A. *Nano Lett.* **2003**, *3*, 1197.
(37) Xu, S.; Mikhailovsky, A. A.; Hollingsworth, J. A.; Klimov, V. I. *Phys. Rev. B* **2002**, *65*, 045319.
(38) Experimental energy-loss rates for highly excited carriers yield an estimate for Γ of around 10 meV.[39]
(39) Norris, D. J.; Nirmal, M.; Murray, C. B.; Sacra, A.; Bawendi, M. G. *Z. Phys. D* **1993**, *26*, 355.
(40) In eq 1, $|M^{tot}|^2 = |M^{surf} + M^{vol}|^2 = |M^{surf}|^2 + |M^{vol}|^2 + (M^{surf})^* \cdot M^{vol} + (M^{vol})^* \cdot M^{surf}$. In Figure 3b, we label $|M^{surf}|^2$ and $|M^{vol}|^2$ as surface and volume contributions, respectively. Because the term $(M^{surf})^* \cdot M^{vol} + (M^{vol})^* \cdot M^{surf}$ is negative and the volume contribution is small, the surface contribution is larger than the total DCM rate.

NL049869W